

PACS numbers: 42.5.Lt; 42.60.By; 41.75.Fr
DOI: 10.1070/QE2015v045n07ABEH015360

Formation of the active medium in high-power repetitively pulsed gas lasers pumped by an electron-beam-controlled discharge

V.D. Bulaev, S.L. Lysenko

Abstract. **A high-power repetitively pulsed e-beam-controlled discharge CO_2 laser is simulated numerically; the simulation results are compared with experimental data. Optimal sizes and design of electrodes and configuration of the external magnetic field are found, which allow one to introduce no less than 90 % electric pump energy into a specified volume of the active medium, including the active volume of a laser with an aperture of 110×110 cm. The results obtained can also be used to design other types of high-power gas lasers.**

Keywords: *high-power repetitively pulsed laser, efficiency, optimisation of electrodes, magnetic corrector.*

1. Introduction

The problem of designing lasers with a high average radiation power still remains urgent. Examples of possible applications of these lasers are discussed in the scientific and technical literature; they include energy transfer at large distances, correction of satellite orbits, removal of space debris from the near-Earth space, launch of artificial satellites, etc. [1–4].

In this paper, based on the results of numerical simulation and existing experimental data, we consider the possibility of designing a high-power electron-beam-controlled (EBC) repetitively pulsed CO_2 laser according to the 'master oscillator–amplifier' scheme [5, 6] and analyse its parameters and characteristics.

Stable lasing in these lasers is obtained by applying a closed cycle of laser mixture circulation and a system for regeneration of a spent laser mixture. A high-power EBC repetitively pulsed CO_2 laser can operate for several hundreds of seconds without any hazardous effect on the environment.

The development of high-power EBC repetitively pulsed CO_2 lasers with an efficiency close to the theoretical limit is hindered by scattering of fast electrons from the accelerator from the foil, foil supports and cathode grid of the laser chamber; diffusion of electrons in the active medium; etc. In this context, the volume of the discharge burning region exceeds significantly the specified volume where laser radiation must be generated; in addition, instabilities arise in the discharge, which violate the bulk burning mode, reduce power and may even suppress lasing.

V.D. Bulaev, S.L. Lysenko State Scientific-Research Test Laser Centre 'Raduga', Raduzhnyi, Vladimir region, 600910 Russia; e-mail: raduga@trassa.org

Received 2 December 2013; revision received 19 May 2014
Kvantovaya Elektronika **45** (7) 610–616 (2015)
Translated by Yu.P. Sin'kov

When studying gas lasers, some researchers sought for optimal solutions using different designs of electrodes (see, e.g., [7–11]), magnetic correctors [12] and beam-limiting devices [13]. However, neither these efforts nor complex study and optimisation of high-power EBC CO_2 lasers [14–18] made it possible to solve completely the problem, i.e., to design a wide-aperture EBC laser with a pumped volume completely matched with a cavity volume.

In particular, the electrode sizes in the direction of the laser mixture flow should be minimal to provide fast recovery of parameters after a pump pulse. At the same time, to implement a maximum pumping level and ensure uniform distribution of pump energy throughout the active medium, one should use electrodes of maximum size. Obviously, the acceptable solution should be a compromise.

In this context, the purpose of our study was to optimise the electrode design with simultaneous optimisation of external electric and magnetic fields, using which one can form a specified pumping volume and obtain limiting laser parameters in both pulsed and repetitively pulsed regimes.

The optimisation criterion was chosen to be the efficiency coefficient

$$\zeta = W_V/W_0, \tag{1}$$

where W_V is the pump energy injected into the working (laser) volume V; W_0 is the total pump energy; and

$$V = adl \tag{2}$$

(a is the width of the accelerator output window, d is the interelectrode distance, and l is the length of the laser-chamber electrodes in the direction along the optical axis).

2. Numerical simulation

Numerical simulation was performed using the Dose-B complex program, which models simultaneously the processes of electron beam propagation in accelerators, design elements and discharge chamber under electric and magnetic fields and the formation of spatial distribution of the electric field and secondary-electron current in the discharge chamber. The self-consistent interaction between the accelerated electron beam with the spatial distribution of the electric field in the discharge chamber, determined by the applied potential difference and laser gas mixture conductivity (induced, in turn, by the accelerated electron beam), was taken into account. The program is implemented on a personal computer; it allows one to change promptly the design parameters of an EBC laser.

Figure 1 illustrates the simulation process. An electron beam, accelerated in vacuum, is incident on a thin foil (*1*) at angles determined by the electronic–optical system of the accelerator. When the beam propagates in the foil material, some electrons are absorbed and some are backscattered into vacuum; however, most of electrons pass through the foil and enter a gas medium (*3*).

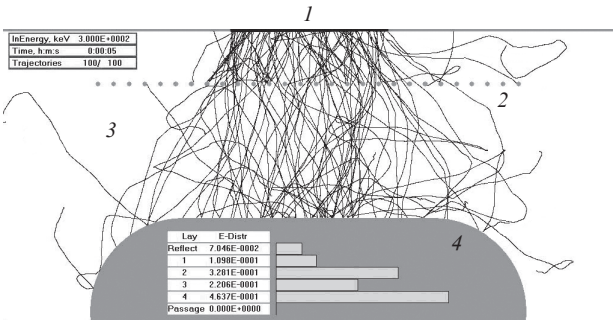

Figure 1. Simulation of electric pumping of an electron-beam-controlled laser:
(*1*) foil; (*2*) cathode grid [(*1*) and (*2*) are cathode elements]; (*3*) gas; (*4*) anode.

The motion of a beam electron was simulated both in the gas and in the design elements (cathode grid, anode, foil) until its energy reduced to 3% of the initial value as a result of inelastic collisions; the energy residue was assumed to be absorbed at the stop point of the electron trajectory. Moving electrons could collide with the cathode grid (*2*) and anode (*4*) or return to the foil; possible absorption and reflection of electrons by design elements was taken into account.

Simulation was performed by the Monte Carlo method, which models three-dimensional motion in arbitrary media [19, 20]; a detailed description of the Dose-B program can be found in [21].

The main mechanisms of electron annihilation are dissociative recombination and attachment. The dependences of dissociative recombination and attachment coefficients on the electric field strength were taken from [22], where they were obtained for the $CO_2 : N_2 : He = 1 : 5 : 4$ mixture.

Using the data on the recombination and attachment rates and solving the stationary kinetic equation, we find the secondary-electron concentration n_e in the electron-beam plasma (EBP) (as in [22]):

$$n_e = \frac{-\beta + \sqrt{\beta^2 + 4\alpha q}}{2\alpha}, \qquad (3)$$

where α is the dissociative-recombination rate constant; β is the attachment coefficient; and q is the formation rate of secondary electrons per unit volume, which is determined during simulation.

The calculation of the number of electrons absorbed in a unit gas volume during simulation yields the electron accumulation rate Q in unit volume and the space charge eQ per unit volume (e is the elementary charge).

The EBP conductivity was determined using the value of secondary-electron concentration n_e (found by simulation) and the data on the secondary-electron drift rate $v(E)$ [23]. The EBP conductivity allows one to determine (using the charge continuity equation and cathode–anode potential difference) the distribution of potential φ and electric field $\boldsymbol{E}$.

$$\mathrm{div}\boldsymbol{j} = \mathrm{div}(\sigma\boldsymbol{E}) = -\mathrm{div}(\sigma\nabla\varphi) = -eQ, \qquad (4)$$

where $\sigma = en_e v(E)/E$ is the plasma conductivity. This equation was solved by the upper relaxation method [24].

Figures 2–4 present as an example the simulation results for the laser-chamber geometry corresponding to Fig. 1.

The adequacy of the model developed was verified by comparing the simulation results with the data in the literature and the results of the experiments with the laser system described in [5].

Figure 2 shows the calculated and experimental dependences of energy W introduced into the plasma on the initial discharge voltage. The following parameters were used in the calculation: the initial energy of beam electrons, 300 keV; the current of the accelerated electron beam incident on the foil, 13.86 A; the duration of the electron beam current, 10–50 μs; the output window width, 25 cm; and the material of the two-layer foil, Al (30 μm) + Ti (18 μm). The laser-chamber parameters were as follows: the distance from the output window to the cathode grid (an array of 28 tubes 0.8 cm in diameter, located with a step 2.5 cm), 9 cm; the distance from the output accelerator window to the anode, 30 cm; the width of the anode flat part, 40 cm; the anode rounding radius, 15 cm; the depth (size of all elements along the optical axis), 210 cm; and $d = 20$ cm.

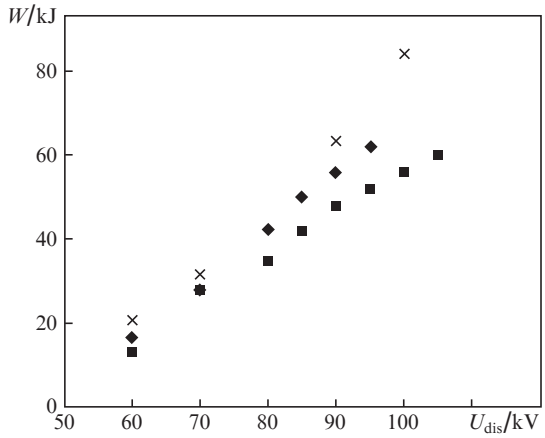

Figure 2. Dependence of the energy injected into plasma on the initial voltage of the capacitor battery: calculation results according to the Dose-B program (×) and experimental results [5] for laser mixtures of gases of special purity grade (◆) and technically pure gases (■).

It can be seen in Fig. 2 that the calculation data coincide (within the measurement errors) with the experimental data for a laser mixture composed of gases of special purity grade.

The calculations were also verified by comparing the results with the data of [7], from which technical and geometric parameters were taken. An example of pump power density distribution over the laser-chamber cross section (based on the data of [7]) is shown in Fig. 3a. Figure 4 presents a calculated gain distribution along the discharge chamber optical axis in comparison with the gain distribution reported in [7] (the discrepancy does not exceed 12%).

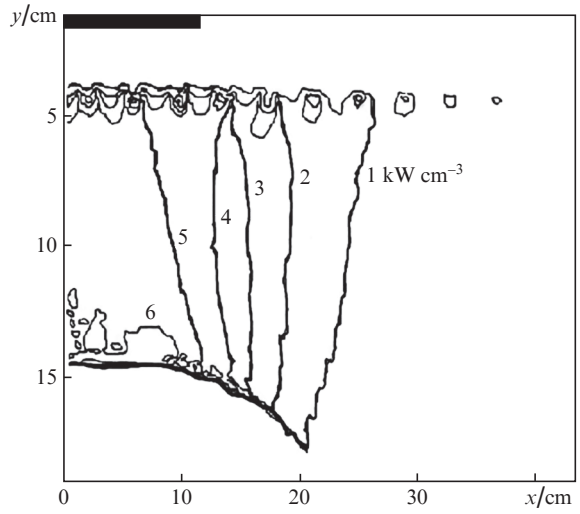

Figure 3. Results of calculating (using the Dose-B program) the right symmetric half of distribution (over the discharge chamber cross section) of the pump power density [7]. The thick horizontal line in the top left corner indicates the accelerator output window.

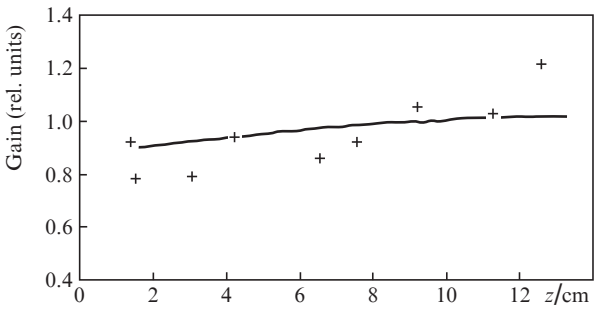

Figure 4. Calculated gain distribution along the z axis of the discharge chamber (solid line) and the gain distribution from [7] (crosses).

It follows from Fig. 3 that the pump energy distribution over the cavity cross section is highly nonuniform; there is a maximum somewhat shifted to the anode.

3. Optimisation of the electrode system

A problem to be solved in design of high-power wide-aperture EBC CO_2 lasers is to implement a high electric field strength in the discharge volume, limited by the cavity aperture, and to form a uniform pump power density distribution in this volume. The experimental results of [5] indicate that the type of electrodes used in [8–11] is not always optimal, because, even in the case of a highly homogeneous electric field in the interelectrode gap, the inhomogeneity of the pump power density in the optical cavity over the discharge cross section may reach 100% (see, for example, Fig. 3 and the results of [7]).

In addition, application of these electrodes does not provide sufficiently high pump levels in both pulsed and repetitively pulsed regimes, because the EBC discharge does not exhibit a direct relationship between an increase in the static breakdown voltage and an increase in the limiting power input [7]. In this context, we used a simplified design of laser-chamber electrodes: each electrode was flat, with cylindrically rounded edges of radius R. The electrode system of the laser chamber must be optimised so as to obtain limiting parameters (laser energy and power) with a maximally possible efficiency coefficient ζ.

Optimisation was performed numerically using the Dose-B program. We calculated electrode systems consisting of a flat cathode grid (the width of which was chosen to be much larger than the interelectrode gap in the laser chamber) and flat anodes with cylindrically rounded edges. Different parameters were varied in numerical experiments: width of the flat part of anodes, rounding radii, interelectrode distance, width of the electron accelerator output window, electron beam parameters (accelerating voltage and current), thickness and material of the accelerator separate foil, etc.

The main simulation result is as follows: all other factors being equal, the decisive parameters are the width of the anode flat part, x_a; the width of the accelerator output window, a; and the interelectrode gap d. The dependence of the power input W to discharge on these parameters can be approximated by the expressions

$$\left.\begin{aligned} W_0 &= W_r^0 + (W_{max} - W_r^0)\left[1 - \exp\left(-\frac{x_a}{a}\right)\right] \\ W_V &= W_V^0 + (W_{V\max} - W_V^0)\left[1 - \exp\left(-\frac{x_a}{a}\right)\right] \end{aligned}\right\} \text{ at } a \geqslant d, \quad (5)$$

$$\left.\begin{aligned} W_0 &= W_r^0 + (W_{max} - W_r^0)\left[1 - \exp\left(-\frac{x_a}{d}\right)\right] \\ W_V &= W_V^0 + (W_{V\max} - W_V^0)\left[1 - \exp\left(-\frac{x_a}{d}\right)\right] \end{aligned}\right\} \text{ at } a < d. \quad (6)$$

Here, W_0 is the total power input; W_V is the power input to the working volume V; W_r^0 and W_V^0 are, respectively, the total power input and the power input to the working volume at $x_a = 0$; and W_{max} and $W_{V\max}$ are, respectively, the total power input and the power input to the working volume for an anode with a sufficiently wide flat part.

Figure 5 shows the calculated dependences of the power inputs and pump efficiency coefficient on the width of the anode flat part for the laser-chamber parameters enumerated in Section 1 (the initial discharge voltage is 105 kV). It can be seen that the power input W_V stops increasing at $x_a \sim 40$–50 cm, despite the fact that the total power input W_0 continues to grow. Thus, the optimal ratio for this case is $x_a/a \approx 2{:}1$.

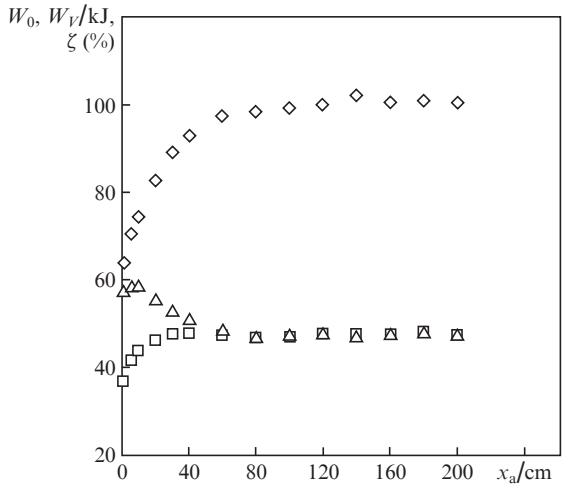

Figure 5. Calculation dependences of (◇) W_0, (□) W_V, and (△) ζ on x_a at $d = 20$ cm.

Similar calculations were performed for different laser mixtures, with variation in the interelectrode gap d and the width of accelerator output window a in the range from 5 to 110 cm; these calculations showed that the x_a/a ratio remains approximately constant (2:1) for all calculation versions, including the variation in the radius R of electrode edge roundings from $d/8$ to d.

The results of the optimisation calculations were confirmed by experiments, in which all laser-chamber parameters, except for the anode design, remained invariable (see Section 2). The first anode version had a flat part 20 cm wide and an edge rounding radius of 11 cm; in the second version, the flat part was 40 cm wide and the rounding radius was 15 cm. The analysis was performed in the repetitively pulsed regime. The results were estimated based on the specific volume pump power [7], determined by the expression

$$q_W = P/G, \tag{7}$$

where $P = Wf$ is the average pump power; W is the pump energy in a pulse; f is the pulse repetition rate; and G is the volume consumption of the laser mixture, measured at the laser-chamber input. A comparison was performed for the maximum attainable q_W values at each frequency; the criterion of pumping stability was the occurrence of no more than 1 or 2 streamer breakdowns in a series of pulses.

Figure 6 shows the results of these comparative experiments. It can be seen that both dependences $q_W(f)$ reach a maximum at the same frequency: $f = 125$ Hz; the increase in q_W for the laser chamber with the second anode is explained by the higher pump energy W in a pulse. Since the lasing efficiency did not change, the rise in the pump power was accompanied by an increase in the average lasing power by more than 30%.

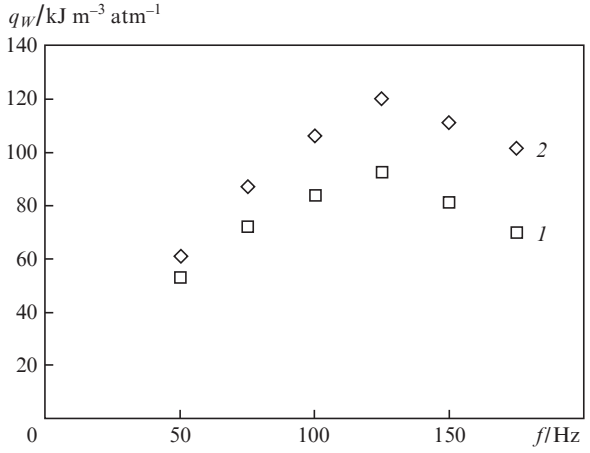

Figure 6. Dependences of the specific volume pump power on the pulse repetition rate: (*1*) anode with a flat part 20 cm wide and rounding radius $R = 11$ cm and (*2*) anode with a flat part 40 cm wide and rounding radius $R = 15$ cm.

Long-term tests of this design of electrodes in the laser system [5] showed that the gas-gap breakdown traces on the anode are on average distributed uniformly over its flat part (Fig. 7), whereas the breakdown traces on the laser-chamber anode in [7] were concentrated in the region of the maximum electric field strength (the central part of the anode).

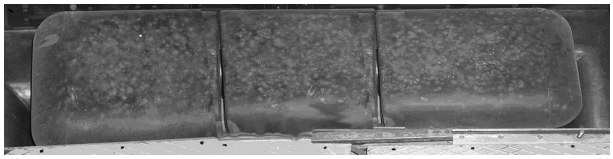

Figure 7. Laser-chamber anode with traces of streamer breakdowns.

Thus, based on the results of numerical simulation and comparative experiments, it was found that the design of flat electrodes with cylindrically rounded edges is optimal. The transverse size of the anode flat part, x_a, must be no less than $2a$ ($a \geqslant d$) or $2d$ ($a < d$).

4. Correction of the pump volume by the external magnetic field

Efficiency ζ can be increased, along with using optimal electrode design, by applying an external axial magnetic field to correct the high-energy electron beam propagation in the laser medium.

This approach was considered both theoretically and experimentally by many authors. For example, calculation results and experimental data on application of solenoids and permanent magnets were reported in [12]; two solenoids were used in [25]; and a special design of electrodes was proposed in [26], where electrodes were composed of miniature resistors with high permeability and high resistivity, with the aid of which the magnetic field of permanent magnets or solenoids was transformed into a field with a specified strength distribution in the interelectrode gap.

However, the problem of optimising the magnetic field parameters and configuration, as well as the design of magnetic forming systems (magnetic correctors), has not been completely solved for wide-aperture EBC lasers.

In this paper, we report the results of studying (based on the Dose-B program) the influence of fields of three types on the EBC CO_2 laser pumping parameters: (i) a uniform magnetic field; (ii) a field formed by a permanent magnet, located under the conducting anode surface; and (iii) a field of a solenoid covering a specified laser volume. Along with a change in the laser-chamber parameters indicated in Section 1, the parameters and configuration of external axial magnetic field of one of these three types were also varied.

Obviously, magnetic correctors based on permanent magnets are most simple to implement. Changing the shape, sizes and position of the magnetic corrector with respect to the electrode system, one can provide a correcting magnetic field to form a specified pumped volume in the best way. At the same time, in the case of a solenoid, the energy necessary to form an equivalent magnetic field configuration is comparable with the laser pump energy [25].

Figure 8 shows an example of electric pumping simulation for a laser chamber with a permanent magnet located under the anode. Figure 9 presents dependences of the pump energy and efficiency coefficient on the magnetic field induction.

It follows from Fig. 9 that the laser chamber in use is characterised by a monotonic rise of W_V with an increase in B from 0 to 0.06 T, with subsequent saturation, and some decrease in W_0 (by ~15% on average). Under these conditions, ζ is almost doubled: from 48% to 90%; i.e., the pump region is almost completely matched with the working volume V.

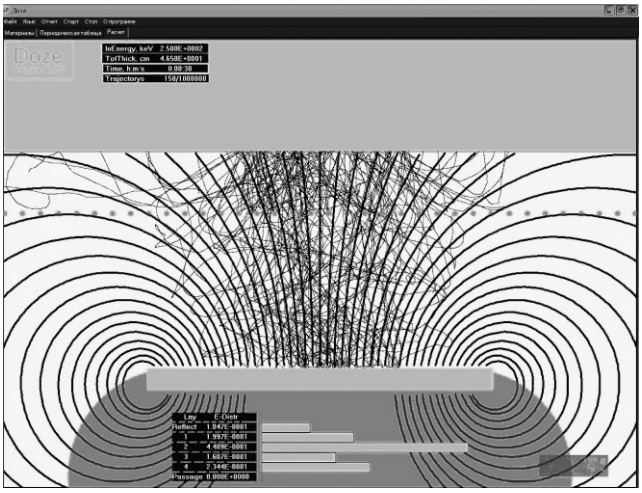

Figure 8. Example of simulated electric pumping for a laser chamber with an axial field induced by a permanent magnet.

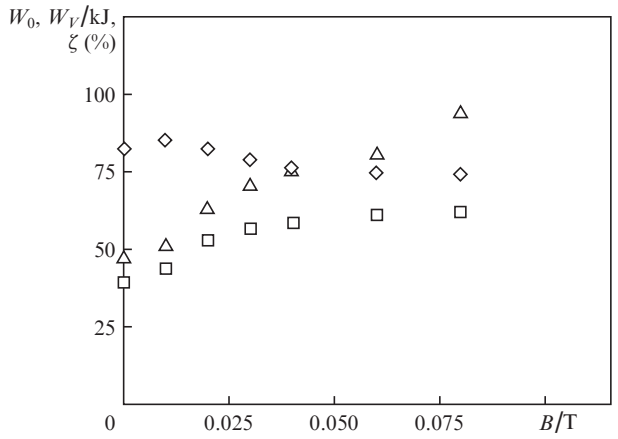

Figure 9. Calculated dependences of the power inputs (◇) W_0 and (□) W_V as well as (△) the efficiency coefficient ζ on the magnetic field induction B. The initial discharge voltage is 100 kV.

The decrease in the total power input W_0 is due to two factors: (1) the magnetic field impedes breakup of the accelerated electron beam, as a result of which the discharge region cross section is reduced, and (2) the decrease in the cross section, in turn, increases the accelerated beam density, ionisation rate q and secondary-electron concentration n_e [see (3)] and, as a consequence, increases the plasma conductivity σ. The discharge gap resistance is inversely proportional to the product of its cross section and the plasma conductivity; hence, the discharge gap resistance increases and the total input power W_0 decreases in stronger magnetic fields.

Calculations of pump regimes with different designs of magnetic correctors based on permanent magnets showed that the optimal solution is a flat permanent magnet located under the conducting anode surface; pumping homogeneity with $\zeta \approx 100\%$ is provided by a flat magnet with a transverse size $x_m \geqslant 2a$.

Thus, the axial field of a permanent magnet not only corrects the trajectories of fast electrons, matching spatially the pumping and lasing regions and, correspondingly, making active-medium ionisation more homogeneous, but also increases the laser efficiency.

5. Discharge chamber of EBC CO_2 laser with maximum attainable parameters

Let us consider the possibility of designing an EBC discharge chamber of a CO_2 laser with maximum attainable parameters.

The possibility of constructing this discharge chamber based on the existing accelerators with electron energy ~300 keV and beam current density $j_e \approx 1-5$ mA cm^{-2}, optimal design of electrodes, and optimal magnetic corrector was modelled using the Dose-B program.

It is known [27] that the energy loss on ionisation for a high-energy electron beam with $E/p > 3.5$ kV cm^{-1} atm^{-1} is compensated for by the electron acceleration in the discharge field; therefore, one can form (with similarity conditions preserved) an EBC discharge in a volume with aperture of ~100×100 cm or larger.

Figure 10 shows an example of simulation of pump energy distribution, and Fig. 11 presents the calculated dependences of the pump energy characteristics for a discharge with E/p = 4 kV cm^{-1} atm^{-1} at electron beam current $I_e = 60$ A, $x_a = 200$ cm, and $l = 210$ cm on the axial magnetic field induction.

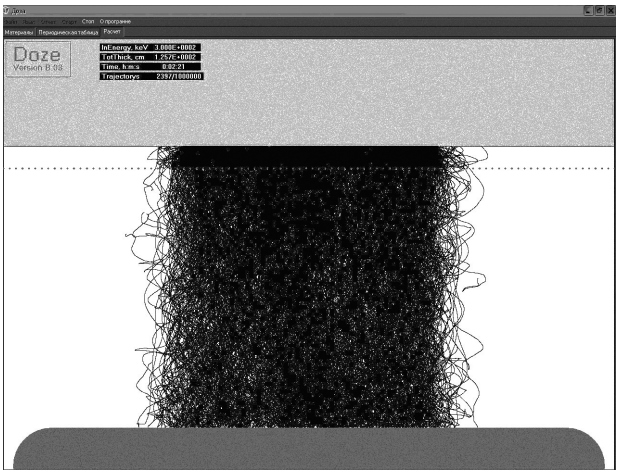

Figure 10. Example of simulated electric-pumping distribution at d = 100 cm, E/p = 4 kV cm^{-1} atm^{-1}, and B = 0.025 T.

It follows from Fig. 11 that that character of the dependences of the pump energy parameters on magnetic field induction is retained at large interelectrode gaps d; however, in contrast to the calculation results for small interelectrode gaps (Figs 5, 9), the decrease in W_0 with an increase in B does not exceed 6%, and acceptable ζ values (95% on average) are attained at much lower inductions B.

Note also that the pumping homogeneity is improved with an increase in the interelectrode gap (Figs 12, 13). The calculation parameters are as follows: the anode–cathode distance 100 cm, the output accelerator window width a = 100 cm, the fast electron energy U_e = 300 keV, the electron beam current $I_e = 60$ A, and the discharge voltage $U = 400$ kV.

An analysis of the results presented in Figs 12 and 13 showed that, all other factors being equal, the optimal input power in the working volume (W_V) is obtained using a permanent magnet with $B = 0.025$ T. In addition, this design of the laser chamber provides a maximum gain on the optical axis; i.e., high efficiency amplifiers (for example, regenerative) can be designed.

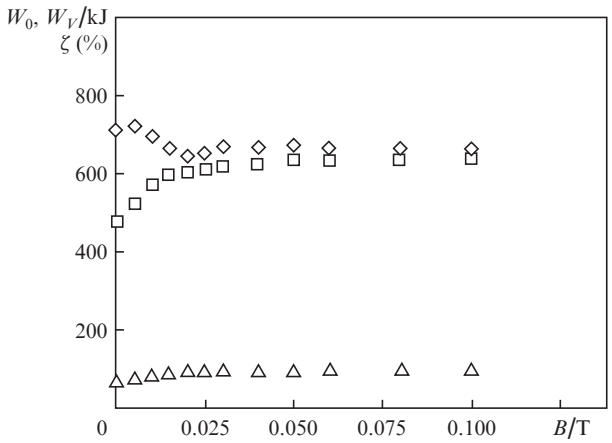

Figure 11. Dependences of (◇) W_0, (□) W_V, and (△) ζ on the magnetic field induction B (d = 100 cm).

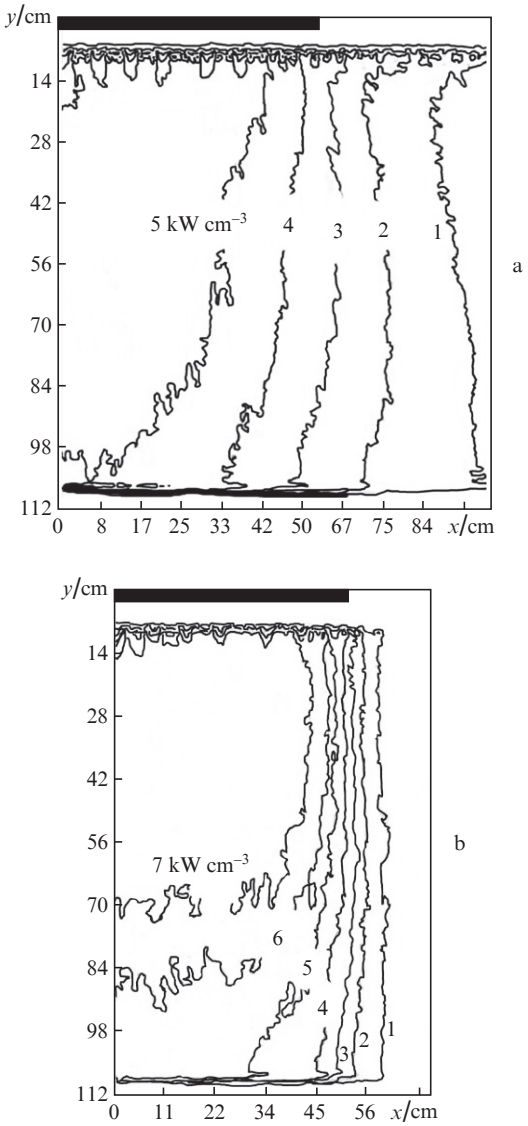

Figure 12. Calculated distribution of pump power density over the discharge chamber cross section at magnetic field inductions B = (a) 0 and (*b*) 0.025 T (d = 100 cm, a = 100 cm, I_e = 60 A, U = 400 kV, and fast electron energy U_e = 300 keV).

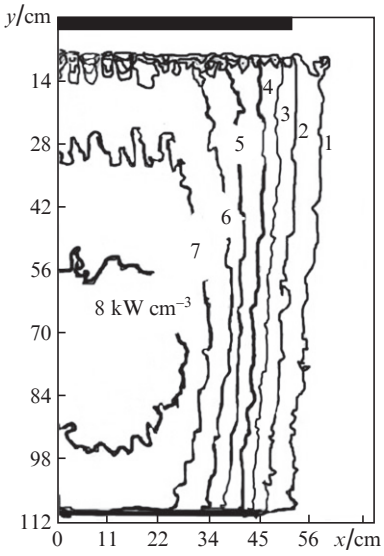

Figure 13. Distribution of the pump power density for the configuration with a magnetic corrector in the form of a permanent magnet with a width x_m = 200 cm and B = 0.025 T; other parameters are as in Fig. 12.

The results of our numerical simulation of the discharge chamber of the EBC CO_2 laser with limiting parameters and the modern state of laser technique show that laser complexes with high average power can be designed in the nearest future.

6. Conclusions

The numerical simulation and experimental study of high-power EBC gas lasers revealed optimal designs of the electrode system and magnetic corrector based on a permanent magnet, with the aid of which a specified pumping volume with efficiency coefficient ζ no less than 90% can be formed in EBC CO_2 lasers.

The laser-chamber anode can be flat, with rounded edges. If the accelerator output window width a is not smaller than the interelectrode gap d ($a \geqslant d$), the acceptable width of the anode flat part is $x_a \approx 2a$, as well as the optimal width of flat magnet, x_m.

Obviously, the final conclusions on the possibility of developing a laser complex with a high average power can be drawn only after experimental verification of the calculation.

The results of this study can be used to design high-power wide-aperture EBC repetitively pulsed lasers of other types, including CO lasers, exciplex (ArF, KrF, etc.) lasers, lasers on atomic transitions in inert gases (ArXe, HeAr), nonchain chemical HF and DF lasers, etc.

References

1. *Proceedings of the First International Symposium on Beamed Energy Propulsion (Huntsville, Alabama, 2002)*. Ed. by A.V. Pakhomov (Melville, New York, 2003).
2. Liukonen R.A., Trofimenko A.M. *Pis'ma Zh. Tekh. Fiz.*, **18** (7), 81 (1992).
3. Rezunkov Yu.A. *Extended Abstract of Doctoral Dissertation* (NIIKI OEPP, Sosnovyi Bor, Leningrad obl., 2006).
4. Apollonov V.V., Tishchenko V.N. *Kvantovaya Elektron.*, **36** (7), 673 (2006) [*Quantum Electron.*, **36** (7), 673 (2006)].
5. Babaev I.K., Bardakovskii S.V., Blinov N.A., et al. *Kvantovaya Elektron.*, **18** (1), 6 (1991) [*Sov. J. Quantum Electron.*, **21** (1), 2 (1991)].

6. Bulaev V.D., Gusev V.S., Zhigan I.P., et al. *AIP Conf. Proc. 3rd Intern. Symp. Beamed Energy Propulsion*, **830**, 361 (2005).
7. Glotov E.P., Danilychev V.A., Cheburkin N.V. *Trudy FIAN*, **142**, 3 (1983).
8. Chang T.J. *Prib. Nauchn. Issled*., **44** (4), 43 (1973).
9. Felici N.J. *Rev. Gen. Elect.*, **59**, 479 (1950).
10. Bruce F.M. *J. Instr. Electr. Eng.*, **94**, 138 (1947).
11. Stappaers E.A. *Appl. Phys. Lett*., **40**, 1018 (1982).
12. Gitt V.D., Pis'mennyi V.D., Rakhimov A.T., et al. *Nesamostoyatel'nyi razryad v magnitnom pole* (Non-Self-Sustaining Discharge in a Magnetic Field) (Moscow: VINITI, 1981).
13. Douglas-Hamilton D.H., Feinberg R.M., Lowder R.S. *J. Appl. Phys.*, **46** (8), 3566 (1975).
14. Bychkov Yu.I., Karlova E.K., Karlov N.V., et al. *Pis'ma Zh. Tekh. Fiz*., **2**, 212 (1976).
15. Datskevich N.P., Karlova E.K., Karlov N.V., et al. *Kvantovaya Elektron*., **4**, 457 (1977) [*Sov. J. Quantum Electron*., **7**, 258 (1977)].
16. Apollonov V.V., Bunkin V.F., Bychkov Yu.I., et al. *Kvantovaya Elektron*., **8**, 1331 (1981) [*Sov. J. Quantum Electron*., **11**, 798 (1981)].
17. Mesyats G.A., Tarasenko V.F. *Kvantovaya Elektron*., **33**, 568 (2003) [*Quantum Electron*., **33**, 568 (2003)].
18. Kovalchuk B.M., Mesyats G.A., Orlovskii V.M., Tarasenko V.F. *Laser Phys.,* **16** (1), 13 (2006).
19. Akkerman A.F. *Modelirovanie traektorii zaryazhennykh chastits v veshchestve* (Simulation of Charged-Particle Trajectories in Matter) (Moscow: Energoatomizdat, 1991).
20. Akkerman A.F., Nikitushev Yu.M., Botvin V.A. *Reshenie metodom Monte-Karlo zadach perenosa bystrykh elektronov v veshchestve* (Solution of Problems of Fast Electron Transport in Matter by the Monte Carlo Method) (Alma-Ata: Nauka, 1972).
21. Bulaev V.D., Lysenko S.L., Danilov S.Yu. *Trudy VIGU*, (7), 92 (2010).
22. Glotov E.P., Danilychev V.A., Kholin I.V. *Trudy FIAN*, **116**, 188 (1980).
23. Grigor'ev I.S., Meilikhov E.Z. (Eds) *Handbook of Physical Quantities* (Boca Raton, FL: CRC Press, 1997; Moscow: Energoatomizdat, 1991).
24. Il'in V.P. *Chislennye metody resheniya zadach elektrofiziki* (Numerical Methods for Solving Problems of Electrophysics) (Moscow: Nauka, 1985).
25. Bakaev V.G., Vadkovskii A.D., Danilov E.O., et al. *Kvantovaya Elektron*., **21** (1), 7 (1994) [*Quantum Electron*., **24** (1), 5 (1994)].
26. Bulaev V.D., Bulaeva O.B. USSR Inventor's Certificate no. 1840810 (1990).
27. Cason C., Perkins I.E., Werkheiser A.H., et al. *AIAA J.*, **15**, 1079 (1977).